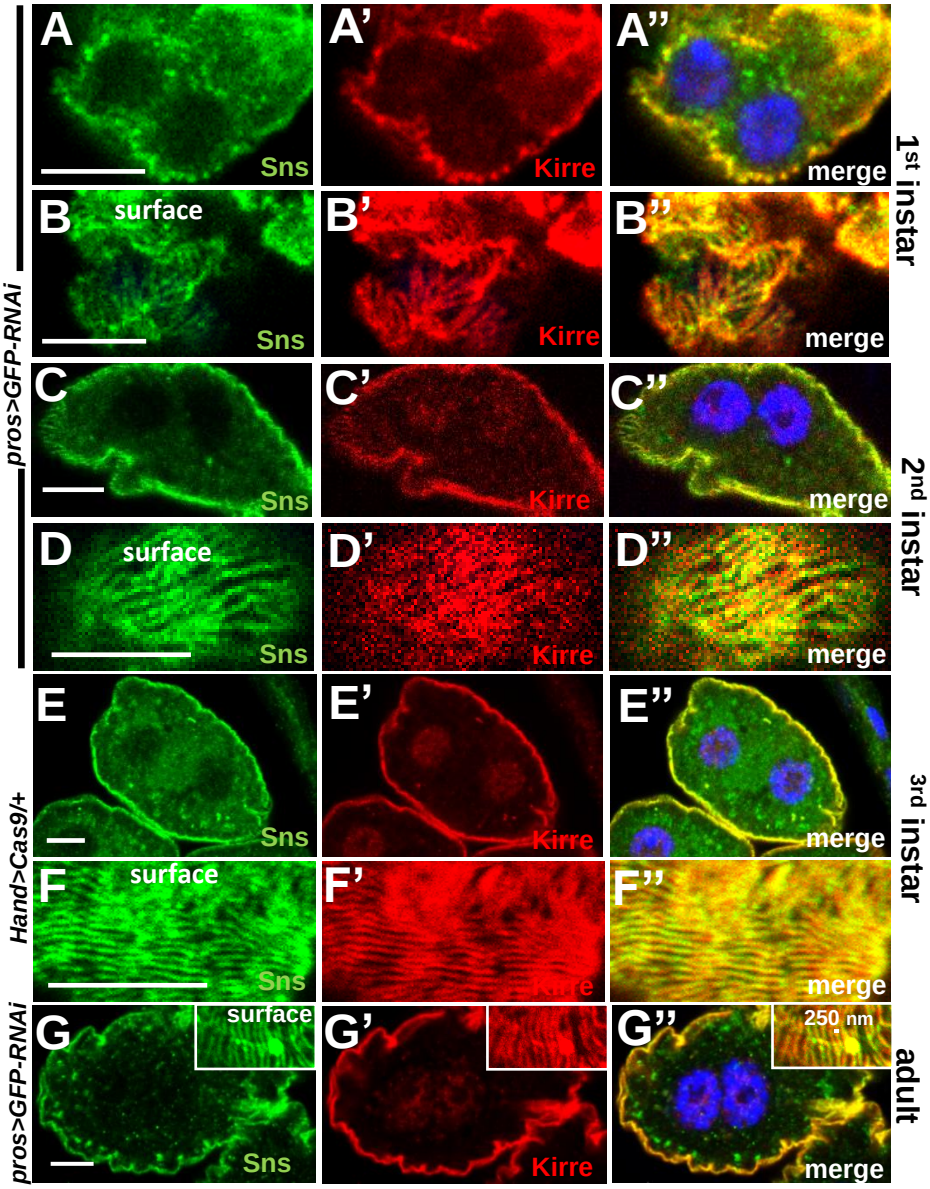

Suppl. Fig. 1. Fingerprint-like pattern of Sns/Kirre is maintained throughout development

(A-B) Control Garland nephrocyte dissected from 1st instar larva and stained for Sns/Kirre. Fingerprint-like pattern is visible as dots in cross section (A-A'') or fine lines on the surface (B-B''). Distance of lines is 250-500 nm.

(C-D) Control Garland nephrocyte dissected from a 2nd instar larva and stained for Sns/Kirre.

(D) Fingerprint-like pattern is visible like in the second instar larval stage.

(E-F'') GCN from 3rd instar larva with expression of *Cas9* driven by *Hand*-GAL4 without expression of gRNA. Sns and Kirre localize towards the cell periphery (E) and a fingerprint-like pattern is detected in the surficial section. This genotype serves as a negative control for CRISPR/Cas9-mediated gene silencing.

(G) Control garland cell nephrocyte dissected from adult animal several days after eclosion. Sns and Kirre are expressed and the fingerprint pattern is maintained

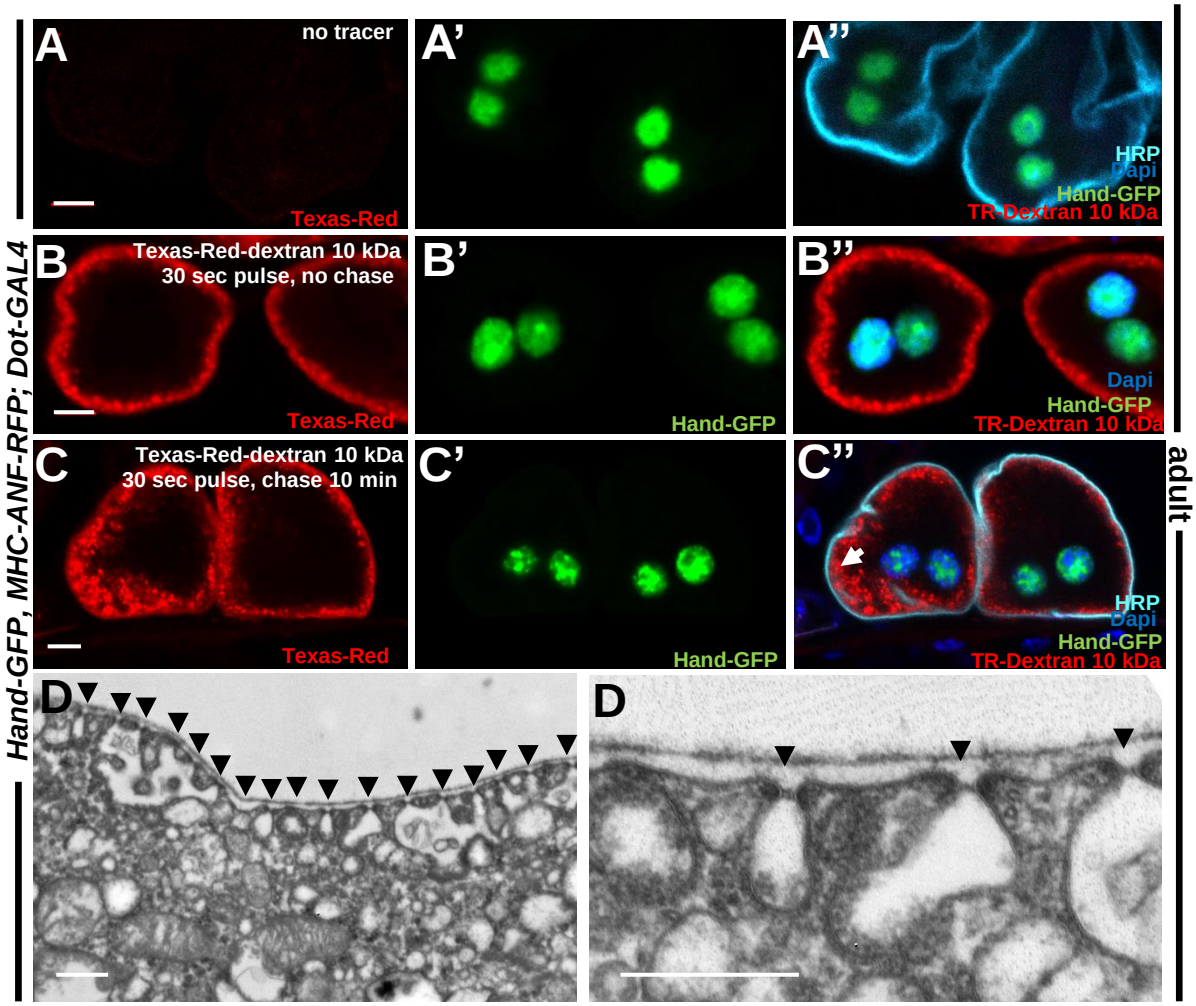

Suppl. Fig. 2. Adult nephrocytes show tracer endocytosis

(A-C) Control Garland nephrocyte dissected from adult animals several days after eclosion. The Hand-GFP, MHC-ANF-RFP;Dot-GAL4 is used as lack of uptake was previously described in this background. The filter set is optimized for Texas-Red but not RFP (endogenous tracer).

(A) The adult GCN are identified by Hand-GFP, HRP and two nuclei as GCN. Without tracer incubation there is no red fluorescence visible.

(B) Exposure for 30 sec to Texas-Red-dextran results in appearance of small red vesicles at the periphery of the cell. This indicates rapid tracer uptake.

(C) The same exposure as in (B) followed by 4 rinses and chasing for 10 min without tracer shows first appearance of vesicles deeper in the cell (arrow). GCN cell membrane is marked by the anti-HRP antibody.

(D) Surface detail of a GCN dissected from adult animal shows typical nephrocyte ultrastructure with slit diaphragms (black arrow heads) and labyrinthine channels.

(E) Magnification from the image in (D). Slit membranes are visible (black arrow heads) and show regular morphology compared to the larval stage (compare Fig. 1D).

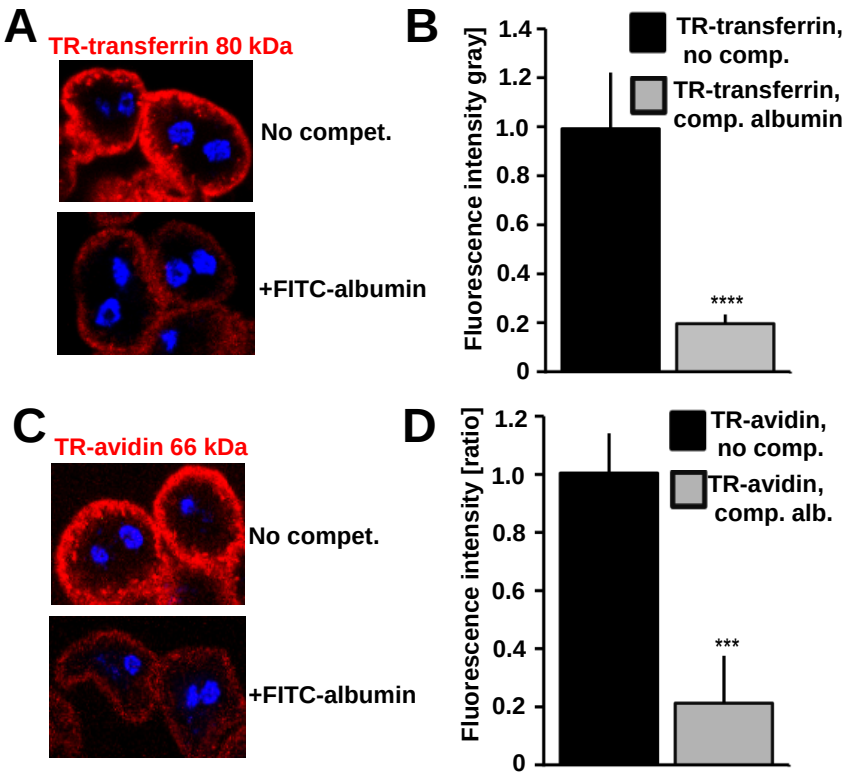

Suppl. Fig. 3. Albumin out-competes uptake of transferrin and avidin.

(A) Control Garland nephrocytes incubated for 5 min with 3 µM Texas-Red-transferrin alone (upper panel) or in presence of an excess of 30 µM FITC-albumin (lower panel). Uptake of Texas-Red-transferrin is strongly reduced by competition.

(B) Quantitation of fluorescence from (A). N=3 per intervention.

(C) Control Garland nephrocytes incubated for 5 min with 3 µM Texas-Red-avidin (3 µM) alone (upper panel) or in presence of an excess of 30 µM FITC-albumin (lower panel). Uptake of Texas-Red-avidin is strongly reduced by competition.

(D) Quantitation of fluorescence from (C). N=3 per intervention.

Supplementary Table 1. 37 genes that if mutated cause human SRNS and their Drosophila orthologues.

Left column indicates functional group of nephrosis genes (see Suppl. Fig.4) followed by human genes involved in the pathogenesis of nephrotic syndrome, literature reference, human accession number, and the corresponding Drosophila orthologue. Orthologues were identified using BLAST analysis and online tools and the number of potential orthologues was restricted to a single gene. COL4A3, ZO1 and KIRREL/NEPH1 are not published monogenic causes of SRNS in humans. They are included due to previous findings implying their relevance for podocytes and of their orthologues for nephrocytes[6].

CATE-GORY	HUMAN GENE SYMBOL	HUMAN GENE FULL NAME	REFERENCE (1st AUTHOR/ YEAR)	ACCESSION NUMBER	*DROSOPHILA ORTHO-LOGUE*	ORTHOLOGUE FULL NAME	ANNO-TATION SYMBOL
Slit membrane complex	***NPHS1***	NEPHRIN	Kestila/1998[1]	NM_004646.3	***sns***	sticks and stones	CG33141
	KIRREL	KIN OF IRRE-LIKE	Donoviel/2001[2]	NM_018240.5	***kirre***	kin of irre	CG3653
	CD2AP	CD2-ASSOCIATED PROTEIN	Lowik/2007[3]	NM_012120.2	***cindr***	CIN85 and CD2AP orthologue	CG31012
	CRB2	CRUMBS, DROSOPHILA, HOMOLOG OF, 2	Ebarasi/2015[4]	NM_173689.5	***crb***	crumbs	CG6383
	FAT1	FAT TUMOR SUPPRESSOR, DROSOPHILA, HOMOLOG OF, 1	Gee/2016[5]	NM_005245.3	***ft***	fat	CG3352
	NPHS2	PODOCIN	Boute/2000[6]	NM_014625.2	***Mec2***	Mec2	CG7635
	DGKE	DIACYLGLYCEROL KINASE, EPSILON, 64-KD	Ozaltin/2013[7]	NM_003647.2	***Dgkε***	Diacyl glycerol kinase ε	CG8657
	PTPRO	PROTEIN-TYROSINE PHOSPHATASE, RECEPTOR-TYPE, O	Ozaltin/2011[8]	NM_030667.2	***Ptp10D***	Protein tyrosine phosphatase 10D	CG1817
	TJP 1	TIGHT JUNCTION PROTEIN 1	(Huber/2003[9])	NM_003257.4	***pyd***	polychaetoid	CG43140
ECM inter-action	***COL4A3***	COLLAGEN, TYPE IV, ALPHA-3	(Malone/2014[10])	NM_000091.4	***vkg***	Viking	CG16858
	ITGA3	INTEGRIN, ALPHA-3	Has/2012[11]	NM_005501.2	***mew***	multiple edematous wings	CG1771
	ITGB4	INTEGRIN, BETA-4	Kambham/2000[12]	NM_000213.3	***mys***	myospheroid	CG1560
	LAMB2	LAMININ, BETA-2	Zenker/2004[13]	NM_002292.3	***LanB1***	LanB1	CG7123
CoQ_{10}	***ADCK4***	AARF DOMAIN-CONTAINING KINASE 4	Ashraf/2013[14]	NM_024876.3	***CG32649***	NN	CG32649
	COQ2	COQ2, S. CEREVISIAE, HOMOLOG OF	Diomedi-Camassei/2007[15]	NM_015697.7	***Coq2***	Coenzyme Q biosynthesis protein 2	CG9613
	COQ6	COQ6, S. CEREVISIAE, HOMOLOG OF	Heeringa/2011[16]	NM_182476.2	***CG7277***	NN	*CG7277*
	PDSS2	PRENYL DIPHOSPHATE SYNTHASE, SUBUNIT 2	Lopez/2006[17]	NM_020381.3	***CG10585***	NN	*CG10585*
Actin regulation	***ACTN4***	ACTININ, ALPHA-4	Kaplan/2000[18]	NM_004924.4	***Actn***	α actinin	CG4376
	ANLN	ACTIN-BINDING PROTEIN ANILLIN	Gbadegesin/2014[19]	NM_018685.2	***scra***	scraps	CG2092
	ARHGAP24	RHO GTPase-ACTIVATING PROTEIN 24	Akilesh/2011[20]	NM_001025616.2	***RhoGAP92B***	Rho GTPase activating protein at 92B	CG4755
	ARHGDIA	RHO GDP-DISSOCIATION INHIBITOR ALPHA	Gupta/2013[21]	NM_001185078.1	***RhoGDI***	RhoGDI	CG7823
	INF2	INVERTED FORMIN 2	Brown/2010[22]	NM_022489.3	***form3***	formin 3	CG33556
	KANK 1 KANK2 KANK4	KN MOTIF- AND ANKYRIN REPEAT DOMAIN-CONTAINING PROTEIN 1	Gee/2015[23]	NM_001256876.1 NM_015493.6 NM_181712.4	***Kank***	Kank	CG10249
	MYO1E	MYOSIN IE	Mele/2011[24]	NM_004998.3	***Myo61F***	Myosin 61F	CG9155
	MYH9	NONMUSCLE	Heath/2001[25]	NM_002473.4	***zip***	zipper	CG15792
Endo-cytosis	***CUBN***	CUBILIN	Ovunc/2011[26]	NM_001081.3	***Cubn***	Cubilin ortholog	CG32702
	SCARB2	SCAVENGER RECEPTOR CLASS B, MEMBER 2	Berkovic/2008[27]	NM_005506.3	***emp***	epithelial membrane protein	CG2727
Trans-criptional regulation	***SMARCAL1***	ASSOCIATED, ACTIN-DEPENDENT REGULATOR OF CHROMATIN, SUBFAMILY A-LIKE PROTEIN 1	Boerkoel/2002[28]	NM_014140.3	***Marcal1***	Marcal1	CG3753
	LMX1B	LIM HOMEOBOX TRANSCRIPTION FACTOR 1, BETA	Vollrath/1998[29]	NM_00117414.1	***CG32105***	NN	*CG32105*
No orthologous gene identified	***PLCE1***	PHOSPHOLIPASE C, EPSILON-1	Hinkes/2006[30]	NM_016341.3			
	EMP2	EPITHELIAL MEMBRANE PROTEIN 2	Gee/2014[31]	NM_001424.4			
	WDR73	WD REPEAT-CONTAINING PROTEIN 73	Colin/2014[32]	NM_032856.2			
	CFH	COMPLEMENT FACTOR H	Sethi/2012[33]	NM_000186.3			
	WT1	WILMS TUMOR 1	Jeanpierre/1998[34]	NM_024426.4			
	MTTL1	TRANSFER RNA, MITOCHONDRIAL, LEUCINE, 1;	Yasukawa/2000[35]	NC_012920.1			

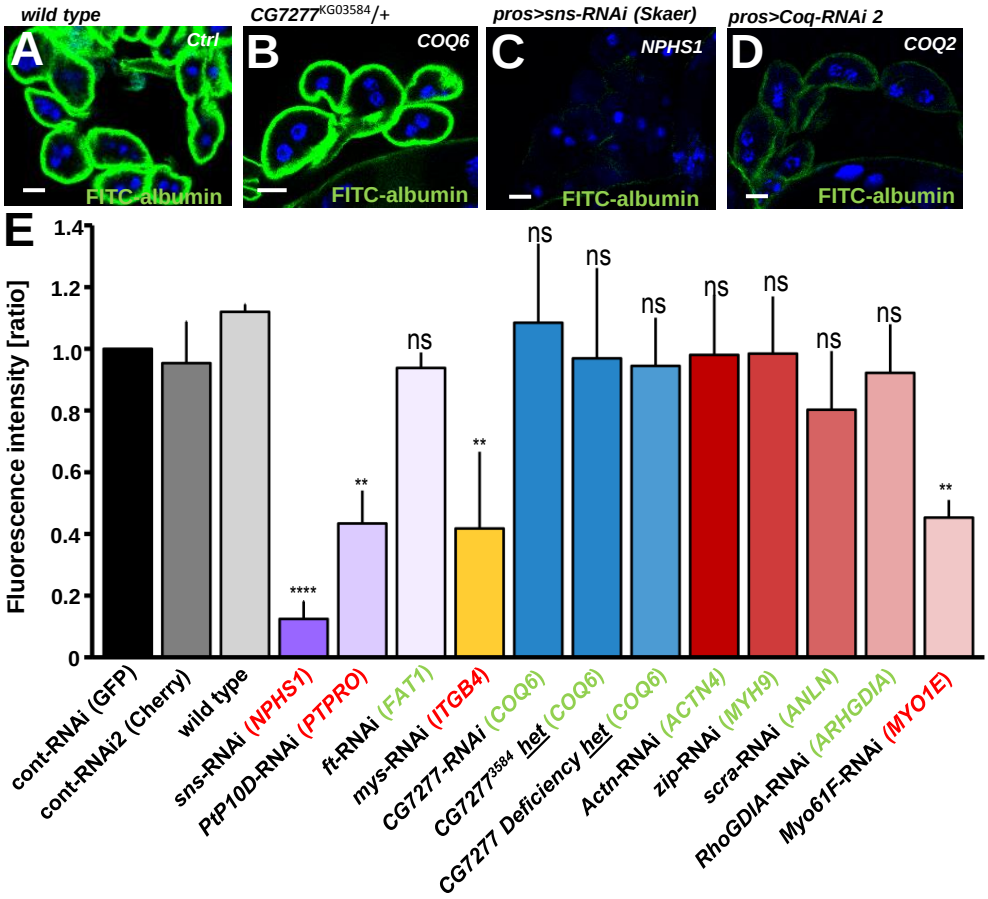

Suppl. Fig. 4. Additional FITC-albumin uptake experiments.

(A-D) Shown are examples FITC-albumin uptake after 30 sec exposure of wild type GCN (A) and GCN *heterozygous* for CG7277^{KG03584} over a wild type chromosome (B). Robust robust FITC-albumin endocytosis can be observed in both genotypes. GCN expressing RNAi directed against *sns* (B), and a second RNAi directed against Coq2 show reduced FITC-albumin uptake. All scale bars represent 10 µm.

(E) Quantitation of fluorescent intensity for genotypes as indicated compared normalized to GFP-RNAi (N=3 per intervention). Human orthologue is denoted in brackets, red letters indicate signficantly reduced FITC-albumin endocytosis, green letters indicate no significant effect (may diverge from the two further RNAi shown in Fig. 3). The allele and deficiency affecting the orthologue of *COQ6* are *heterozygous* over a wild type chromosome. Statistical significance was calculated using ANOVA and Dunnet's post hoc analysis.

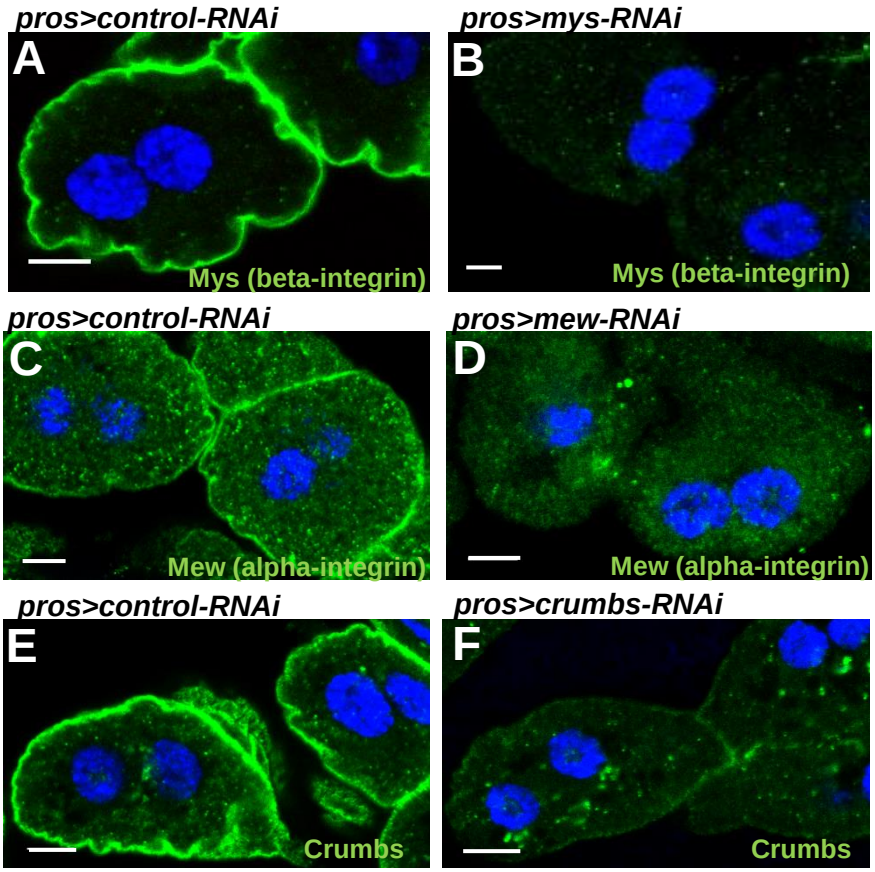

Suppl. Fig. 5. Knock-down efficiency tested by Immunofluorescence.
(A-F) All images are recorded with identical settings for control and knockdown.
(A) GCN expressing control RNAi stained for the orthologue of *ITGB4*.

(B) Silencing of the orthologue of ITGBA strongly reduces signal of the anti-mys antibody suggesting efficient knockdown.

(C) GCN expressing control RNAi stained for the orthologue of *ITGA3*.

(D) Silencing of the orthologue of ITGBA strongly reduces signal of the anti-mew antibody suggesting efficient knockdown.

(E) GCN expressing control RNAi stained for the orthologue of *CRB2*.

(F) Silencing of the orthologue of *CRB2* strongly reduces signal of the anti-crumbs antibody suggesting efficient knockdown.

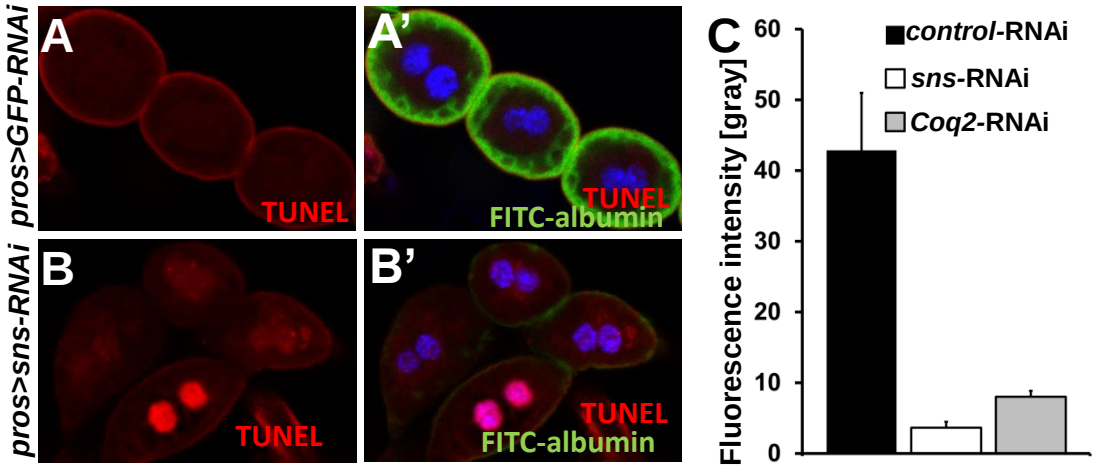

Supplementary Fig. 6. Uptake of TUNEL-negative cells is strongly affected upon knockdown of *sns* and *Coq2*.
(A-A') Control garland cell nephrocytes are TUNEL-negative and show strong uptake of FITC-albumin. **(B-B')** Silencing *sns* results in the appearance of TUNEL-positive nephrocytes like the cell below in the middle of the representative image. TUNEL-negative and TUNEL-positive cells alike show a reduced uptake of FITC-albumin. **(C)** Quantitation of FITC-albumin-uptake using Image J for TUNEL-negative cells expressing control-RNAi (EGFP-RNAi) or RNAis directed against *sns* or *Coq2 (*N= 3 animals for each genotype).

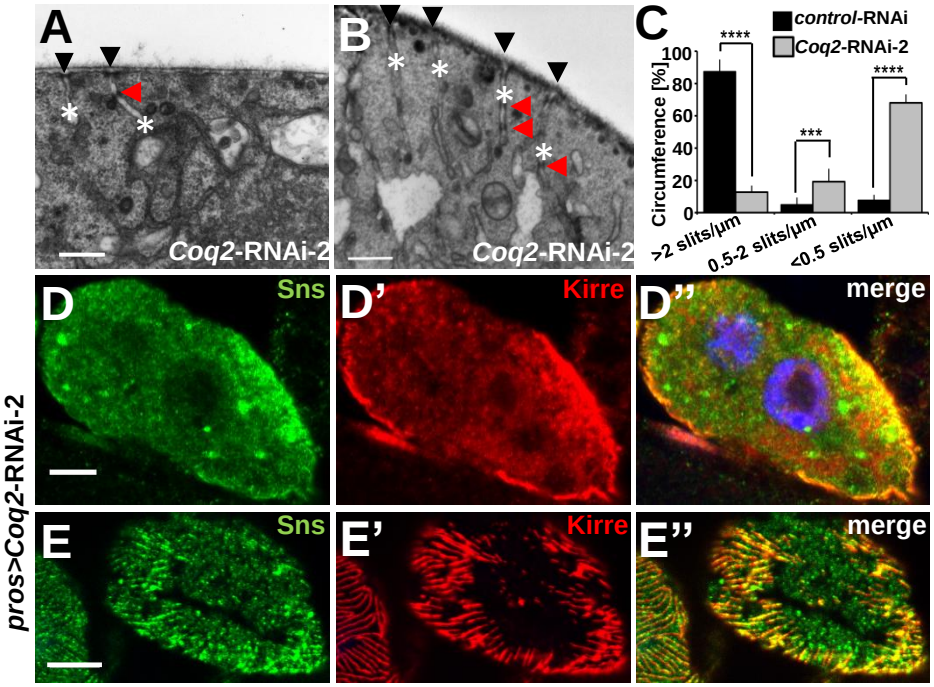

Supplementary. Fig. 7. *Coq2*-RNAi findings are confirmed by a second RNAi-line.

(A-B) EM-images of nephrocytes expressing a second Coq2-RNAi show reduced number of SDs (arrow heads) and labyrinthine channels (asterisks). SDs are often mislocalized into the labyrinthine channels and multiplied (red arrow heads).

(C) Quantitation of frequency of SD measured along one complete GNC diameter for control-RNAi compared to Coq2-RNAi as mean of 6 cells from 3 different animals. Frequency of SDs was classified into three groups: normal (>2 slits/µm), reduced (0.5-2 slits/µm) and sporadic (<0.5 slits/µm). Note the strong reduction of SDs in Coq2-RNAi.

(D-D") Immunostaining of Sns/Kirre in Garlands expressing *Coq2*-RNAi2 reveals gaps and partial misplacement of Sns/Kirre from the membrane.

(E-E") Surface section of nephrocyte expressing *Coq2*-RNAi 2 shows gaps of Sns/Kirre on the surface.

All Scale bars represent 500 nm in electron microscopy images and 5 µm in confocal images.

Supplementary Table 2. Drosophila RNAi lines used in this study.
Drosophila stocks were obtained from from Vienna Drosophila Drosophila Resource Center (VDRC) or Bloomington Drosophila Stock Center at Indiana University (BDSC) unless otherwise indicated. Source ID is noted as Transformant ID (VDRC) or stock number (BDSC). Uptake is denoted as percent of uptake compared to control (GFP-RNAi).

stock name	CG #	source	source ID#	uptake [%]
UAS-EGFP-RNAi	-	BDSC	41553	100
UAS-mCherry-RNAi	-	BDSC	35785	95
UAS-sns-RNAi	*CG33141*	VDRC	109442	10
UAS-sns-RNAi	*CG33141*	BDSC	64872	12
UAS-sns-RNAi	*CG33141*	H. Skaer	-	7
UAS-kirre-RNAi	*CG3653*	VDRC	27227	8
UAS-kirre-RNAi	*CG3653*	VDRC	109585	17
UAS-pyd-RNAi	*CG43140*	BDSC	35225	14
UAS-pyd-RNAi	*CG43140*	BDSC	33386	13
UAS-Mec2-RNAi	*CG7635*	VDRC	104601	57
UAS-Mec2-RNAi	*CG7635*	BDSC	61259	54
UAS-Cindr-RNAi	*CG31012*	BDSC	38328	47
UAS-Cindr-RNAi	*CG31012*	BDSC	38976	54
UAS-crb-RNAi	*CG6383*	BDSC	40869	66
UAS-crb-RNAi	*CG6383*	BDSC	34999	78
UAS-Ptp10D-RNAi	*CG1817*	VDRC	110443	43
UAS-Ptp10D-RNAi	*CG1817*	BDSC	39001	93
UAS-Ptp10D-RNAi	*CG1817*	VDRC	1101	76
UAS-Dgke-RNAi	*CG8657*	VDRC	4659	75
UAS-Dgke-RNAi	*CG8657*	BDSC	57750	83
UAS-ft-RNAi	*CG3352*	VDRC	108863	81
UAS-ft-RNAi	*CG3352*	BDSC	34970	92
UAS-ft-RNAi	*CG3352*	VDRC	9396	94
UAS-LanB1-RNAi	*CG7123*	VDRC	23121	14
UAS-LanB1-RNAi	*CG7123*	BDSC	42616	71
UAS-mys-RNAi	*CG1560*	BDSC	33642	51
UAS-mys-RNAi	*CG1560*	VDRC	29619	19
UAS-mys-RNAi	*CG1560*	BDSC	27735	42
UAS-mew-RNAi	*CG1771*	BDSC	44553	47
UAS-mew-RNAi	*CG1771*	BDSC	27543	54
UAS-vkg-RNAi	*CG16858*	BDSC	50895	57
UAS-vkg-RNAi	*CG16858*	VDRC	106812	47
UAS-Coq2-RNAi	*CG9613*	BDSC	27054	13
UAS-Coq2-RNAi (2)	*CG9613*	VDRC	108373	34
UAS-CG32649-RNAi	*CG32649*	VDRC	110801	12
UAS-CG32649-RNAi	*CG32649*	BDSC	57039	46
UAS-CG7277-RNAi	*CG7277*	VDRC	30693	108
CG7277^{KG03584}/Def	*CG7277*	BDSC	13964/9602	53
CG7277^{KG03584} hom	*CG7277*	BDSC	13964	31
CG7277^{KG03584}/+	*CG7277*	BDSC	13964	97
CG7277 Deficiency/+	*CG7277*	BDSC	9602	94
UAS-CG10585-RNAi	*CG10585*	VDRC	110196	69
UAS-CG10585-RNAi	*CG10585*	BDSC	51910	104
UAS-RhoGAP92B-RNAi	*CG4755*	VDRC	105663	45
UAS-RhoGAP92B-RNAi	*CG4755*	BDSC	33391	55
UAS-Kank-RNAi	*CG10249*	BDSC	33432	69
UAS-Kank-RNAi	*CG10249*	VDRC	15009	53
UAS-scra-RNAi	*CG2092*	VDRC	104674	80
UAS-scra-RNAi	*CG2092*	BDSC	53358	39
UAS-scra-RNAi	*CG2092*	VDRC	33465	59
UAS-RhoGDI-RNAi	*CG7823*	VDRC	105765	94
UAS-RhoGDI-RNAi	*CG7823*	VDRC	46154	76
UAS-RhoGDI-RNAi	*CG7823*	BDSC	40902	92
UAS-zip-RNAi	*CG3533*	VDRC	104208	98
UAS-zip-RNAi	*CG3533*	BDSC	36727	48
UAS-zip-RNAi	*CG3533*	BDSC	38259	52
UAS-Myo61F-RNAi	*CG9155*	VDRC	110682	101
UAS-Myo61F-RNAi	*CG9155*	BDSC	41689	82
UAS-Myo61F-RNAi	*CG9155*	VDRC	49345	45
UAS-Actn-RNAi	*CG4376*	BDSC	34874	98
UAS-Actn-RNAi	*CG4376*	VDRC	7762	22
UAS-Actn-RNAi	*CG4376*	VDRC	110719	49
UAS-form3-RNAi	*CG33556*	VDRC	45594	105
UAS-form3-RNAi	*CG33556*	VDRC	42302	92
UAS-Marcal1-RNAi	*CG3753*	VDRC	34701	55
UAS-Marcal1-RNAi	*CG3753*	BDSC	33709	64
UAS-CG32105-RNAi	*CG32105*	VDRC	108747	113
UAS-CG32105-RNAi	*CG32105*	VDRC	51269	87
UAS-Cubn-RNAi	*CG32702*	BDSC	51736	4
UAS-Cubn-RNAi	*CG32702*	BDSC	28702	4
UAS-emp-RNAi	*CG2727*	VDRC	12233	118
UAS-emp-RNAi	*CG2727*	BDSC	40947	40
UAS-ND75-RNAi	*CG2286*	BDSC	33910	30
UAS-ND75-RNAi	*CG2286*	BDSC	33911	53
UAS-mgl-RNAi	*CG42611*	BDSC	33940	73
UAS-mgl-RNAi	*CG42611*	VDRC	105071	71
UAS-Amnionless-RNAi	*CG11592*	VDRC	104099	1
UAS-Amnionless-RNAi	*CG11592*	BDSC	41956	3